Inorg. Chem. **2008**, *47*, 2534−2542

Tris(phosphino)borato Silver(I) Complexes as Precursors for Metallic Silver Aerosol-Assisted Chemical Vapor Deposition

Matthew N. McCain,[†] Sven Schneider,[‡] Michael R. Salata,[†] and Tobin J. Marks*[,†]

Department of Chemistry and the Materials Research Center, Northwestern University, 2145, Sheridan Road, Evanston, Illinois 60208-3113

Received September 19, 2007

A series of light- and air-stable tris(phosphino)borato silver(I) complexes has been synthesized, structurally and spectroscopically characterized, and implemented in the growth of low resistivity metallic silver thin films by aerosol-assisted chemical vapor deposition (AACVD). Of the four complexes in the series, $[RB(CH_2PR'_2)_3]AgPEt_3$ (R = Ph (**1**, **3**), ^{n}Bu (**2**, **4**); R′ = Ph (**1**, **2**), ^{i}Pr (**3**, **4**), complexes **1** and **2** have been characterized by single-crystal X-ray diffraction. Complex **2** represents a significant improvement over previously available nonfluorinated Ag precursors, owing to ease of handling and efficient film deposition characteristics. Thermogravimetric analysis (TGA) shows that the thermolytic properties of these complexes can be significantly modified by altering the ligand structure. Polycrystalline cubic-phase Ag thin films were grown on glass, MgO(100), and 52100 steel substrates. Ag films of thicknesses 3 μm, grown at rates of 14–18 nm/min, exhibit low levels of extraneous element contamination by X-ray photoelectron spectroscopy (XPS). Atomic force microscopy (AFM) and scanning electron microscopy (SEM) indicate that film growth proceeds primarily via an island growth (Volmer–Weber) mechanism.

Introduction

Metallic silver thin films have importance in a wide range of applications including microelectronics as advanced interconnects,[1] components of high T_c superconductor structures for improved stress durability,[2] and friction and wear control via solid lubricant coatings.[3] Various methods have been used to deposit silver thin films, such as sputtering,[4] thermal evaporation,[5] electron-beam evaporation,[6] and chemical vapor deposition (CVD).[7] Of these techniques, CVD processes offer the attraction of conformal surface coverage at closer to ambient conditions, adaptability to a wide range of materials and manufacturing scales, simple apparatus, and the possibility of creating metastable phases. For the deposition of metallic thin films, metal-organic (MO) CVD has

* E-mail: t-marks@northwestern.edu.
† Northwestern University.
‡ Current address: Technische Universität München, Anorganisch-Chemisches Institut, Lichtenbergstrasse 4, 85747 Garching, Germany.

(1) (a) Gao, L.; Harter, P.; Linsmeier, Ch.; Wiltner, A.; Emling, R.; Schmitt-Landsiedel, D. *Microelectron. Eng.* **2005**, *82*, 296–300. (b) Shacham-Diamand, Y.; Inberg, A.; Sverdlov, Y.; Croitoru, N. *J. Electrochem. Soc.* **2000**, *147*, 3345–3349. (c) Manepalli, R.; Stepniak, F.; Bidstrup-Allen, S. A.; Kohl, P. A. *IEEE Trans. Adv. Packag.* **1999**, *22*, 4–8.

(2) (a) Iida, K.; Kaneko, T.; Katagiri, K.; Sakai, N.; Murakami, M.; Koshikuza, N. *Supercond. Sci. Technol.* **2004**, *17*, S46–S50. (b) Harnois, C.; Desgardin, G.; Laffez, I.; Chaud, X.; Bourgault, D. *Physica C* **2002**, *383*, 269–278. (c) Kalyanaraman, R.; Oktyabrsky, S.; Narayan, J. *J. Appl. Phys.* **1999**, *85*, 6636–6641.

(3) (a) DellaCorte, C.; Edmonds, B. J. *NASA Tech. Memo.* **1995**, 107056. (b) DellaCorte, C.; Pepper, S. V.; Honecy, F. S. *Surf. Coat. Technol.* **1992**, *52*, 31–37. (c) Erdemir, A.; Fenske, G. R.; Nichols, F. A.; Erck, R. A. *Tribol. Trans.* **1990**, *33*, 511–518. (d) DellaCorte, C.; Sliney, H. E.; Deadmore, D. L. *Tribol. Trans.* **1988**, *31*, 329–334.

(4) Hauder, M.; Hansch, W.; Gstootner, J.; Schmitt-Landsiedel, D. *Appl. Phys. Lett.* **2001**, *78*, 838–840.

(5) Uchil, J.; Mohan Rao, K.; Pattabi, M. *J. Phys. D: Appl. Phys.* **1996**, *29*, 2992–2996.

(6) Carter, A. C.; Chang, W.; Qadri, S. B.; Horwitz, J. S.; Leuchtner, R.; Chrisey, D. B. *J. Mater. Res.* **1998**, *13*, 1418–1421.

(7) (a) Grodzicki, A.; Lakomska, I.; Piszczek, P.; Szymanska, I.; Szlyk, E. *Coord. Chem. Rev.* **2005**, *249*, 2232–2258. (b) *The Chemistry of Metal CV*; Kodas, T., Hampden-Smith, M., Eds.; VCH: Weinheim, Germany, 1994.

(8) (a) McCain, M. N.; Metz, A. W.; Yang, Y.; Stern, C. L.; Marks, T. J. *Chem. Vap. Deposition* **2005**, *11*, 291–294. (b) Metz, A. W.; Ireland, J. R.; Zheng, J.-G.; Lobo, Ricardo P. S. M.; Yang, Y.; Ni, J.; Stern, C. L.; Dravid, V. P.; Bontemps, N.; Kannewurf, C. R.; Poeppelmeier, K. R.; Marks, T. J. *J. Am. Chem. Soc.* **2004**, *126*, 8477–8492. (c) Choy, K. L. *Prog. Mater. Sci.* **2003**, *48*, 57–170. (d) Samoilenkov, S.; Stefan, M.; Wahl, G.; Paramonov, S.; Kuzmina, N.; Kaul, A. *Chem. Vap. Deposition* **2002**, *8*, 74–78. (e) Chi, K.-M.; Lu, Y.-H. *Chem. Vap. Deposition* **2001**, *7*, 117–120. (f) Belot, J. A.; Wang, A.; McNeely, R. J.; Liable-Sands, L.; Rheingold, A. L.; Marks, T. J. *Chem. Vap. Deposition* **1999**, *5*, 65–69. (g) Belot, J. A.; Neumayer, D. A.; Reedy, C. J.; Studebaker, D. B.; Hinds, B. J.; Stern, C. L.; Marks, T. J. *Chem. Mater.* **1997**, *9*, 1638. (h) Shulz, D. L.; Marks, T. J. *CVD of Non-Metals* Rees, W., Ed.; VCH: New York, 1996; Vol. *39*, p 150. (i) Schulz, D. L.; Marks, T. J. *Adv. Mater.* **1994**, *6*, 719.

10.1021/ic701852x CCC: $40.75
Published on Web 02/23/2008

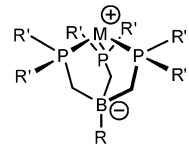

Figure 1. Generalized structure of the family of tris(phosphino)borato low-valence metal complexes.

been widely established.[8] However, a major limitation of this method is the requirement of highly volatile metal-organic precursors. Traditionally, the design of silver precursors has focused mainly on β-diketonates[8e,9] or structurally related ligands,[10] as well as carboxylates,[7a,8d,11] featuring tertiary phosphine ancillary ligands. Without the use of expensive fluorinated substituents, these compounds suffer from poor volatility, as well as from poor stability under ambient conditions. Films deposited using complexes with fluorinated substituents suffer from significant F contamination. In comparison, aerosol-assisted (AA) CVD has been recently developed to utilize metal precursors with lower volatilities, without sacrificing film quality.[7b,8c,12] However, compared to MOCVD, reports of silver thin film growth by AACVD have been limited,[13] with reported precursors also suffering from instability under ambient conditions.

Peters and co-workers have recently developed a family of tris(phosphino)borato ligands (Figure 1) that has been shown to effectively stabilize monomeric complexes of low-valence late transition metals with particularly interesting reactivities toward small molecule activation.[14] The strong tendency of the monoanionic chelate ligand to enforce pseudotetrahedral coordination geometries in combination with the soft phosphorus donors should be ideally suited to form monometallic silver(I) complexes. However, to date, no silver tris(phosphino)borato complexes have been reported. In this contribution, we report the synthesis and structural/spectroscopic characterization of a series of tris(phosphino)borato silver(I) complexes which are both air- and light-stable. The thermal stabilities and decomposition pathways of these complexes are investigated, and their implementation as effective precursors for the growth of metallic silver thin films by AACVD is reported.

Experimental Section

Materials and Methods. All manipulations of air-sensitive materials were carried out with rigorous exclusion of oxygen and moisture in flame- or oven-dried Schlenk-type glassware on a dual-manifold Schlenk line, or in a nitrogen-filled Vacuum Atmospheres or MBraun glovebox with a high-capacity recirculator (<2 ppm O_2). Hydrocarbon solvents (pentane and toluene) were dried using an activated alumina column and Q-5 column according to the method described by Grubbs,[15] or by distilling from calcium hydride (dichloromethane) or sodium (diethyl ether, tetrahyrofuran). Ph_2PCH_3 (ACROS) and all other reagents (Aldrich) were used without further purification. $Ph_2PCH_2Li\cdot TMEDA$,[16] [Li(TMEDA)]-$PhB(CH_2PPh_2)_3$[17] and $^iPrPCH_2Li$[18] were prepared by literature methods. Deuterated solvents (Cambridge Isotope Laboratories) were dried over CaH_2, transferred via filter cannula under inert atmosphere, and stored over 4-A molecular sieves in vacuum-tight storage flasks prior to use.

Physical and Analytical Measurements. Elemental analyses were performed by Midwest Microlabs, Inc. NMR spectra were recorded on a Varian Mercury-400 (FT, 400 MHz, ^{1}H; 100 MHz, ^{13}C, 162 MHz ^{31}P) instrument. ^{1}H and ^{13}C chemical shifts (δ) were referenced to residual solvent. Chemical shifts for ^{31}P are reported relative to an external 85% H_3PO_4 standard at room temperature. Thermogravimetric analysis (TGA) was performed on a Mettler Toledo TGA/SDTA851^e ultramicro balance instrument at a ramp rate of 2.5 °C min^{-1} and under a N_2 flow rate of 50 mL min^{-1} at atmospheric pressure.

Synthesis of [PhB(CH$_2$PPh$_2$)$_3$Ag(PEt$_3$)] (1). Using a mortar and pestle, 0.29 g (2.0 mmol) AgCl was ground to a fine powder and added to a 100 mL flask containing 1.62 g (2.0 mmol) of $[Li(TMEDA)PhB(CH_2PPh_2)_3]$. The flask was evacuated and backfilled with N_2 three times, covered with aluminum foil, and cooled to −78 °C in an acetone/dry ice bath. After tetrahydrofuran (45 mL) was added, 0.30 g (2.0 mmol) of triethylphosphine was added via syringe. The reaction mixture was stirred for 30 min and then removed from the cooling bath and allowed to warm to room temperature with stirring. The yellow solution was next separated from the colorless solids via cannula filtration into another Schlenk flask. The solvent was removed in vacuo and the residue washed with 3 × 60 mL of pentane (vigorous stirring) to remove TMEDA. The solid residue was then dissolved with 60 mL toluene and the resulting yellow solution filtered from colorless solids via cannula.

(9) (a) Paramonov, S.; Samoilenkov, S.; Papucha, S.; Malkerova, I.; Alikhanyan, A.; Kuzmina, N.; Troyanov, S. I.; Kaul, A. R. *J. Phys. IV* **2001**, *11*, Pr3645–Pr3652. (b) Chi, K.-M.; Lin, C.-T.; Peng S.-M.; Lee, G.-H. *Organometallics,* **1996**, *15*, 2660–2663. (c) Yuan, Z.; Dryden, N. H.; Li, X.; Vittal, J. J.; Puddephatt, R. J. *J. Mater. Chem.* **1995**, *5*, 303–7. (d) Yuan, Z.; Dryden, N. H.; Vittal, J. J.; Puddephatt, R. J. **1995**, *7*, 1696–702. (e) Serghini-Monim, S.; Yuan, Z.; Griffiths, K.; Norton, P. R.; Puddephatt, R. J. *J. Am. Chem. Soc.* **1995**, *117*, 4030–4036. (f) Xu, C.; Corbitt, T. S.; Hampden-Smith, M. J.; Kodas, T. T.; Duesler, E. N. *J. Chem. Soc., Dalton Trans.* **1994**, *19*, 2841–9. (g) Dryden, N. H.; Vittal, J. J.; Puddephatt, Richard J. *Chem. Mater.* **1993**, *5*, 765–6.

(10) (a) Ngo, S. C.; Banger, K. K.; Toscano, P. J.; Welch, J. T. *Polyhedron* **2002**, *21*, 1289–1297. (b) Edwards, D. A.; Harker, R. M.; Mahon, M. F.; Molloy, K. C. *J. Mater. Chem.* **1999**, *9*, 1771–1780.

(11) (a) Haase, T.; Kohse-Hoeinghaus, K.; Atakan, B.; Schmidt, H.; Lang, H. *Chem. Vap. Deposition* **2003**, *9*, 144–148. (b) Szlyk, E.; Piszczek, P.; Grodzicki, A.; Chaberski, M.; Golinski, A.; Szatkowski, J.; Blaszczyk, T. *Chem. Vap. Deposition* **2001**, *7*, 111–116. (c) Lu S.-Y.; Lin, Y.-Z. *Thin Solid Films* **2000**, *376*, 67–72. (d) Szlyk, E.; Piszczek, P.; Lakomska, I.; Grodzicki, A.; Szatkowski, J.; Blaszczyk, T. *Chem. Vap. Deposition* **2000**, *6*, 105–108.

(12) (a) Rodriquez-Castro, J.; Mahon, M. F.; Molloy, K. C. *Chem. Vap. Deposition* **2006**, *12*, 601–607. (b) Peters, E. S.; Carmalt, C. J.; Parkin, I. P.; Tocher, D. A. *Eur. J. Inorg. Chem.* **2005**, *4179*, 4185. (c) Schäfer, P.; Waser, R. *Adv. Mater. Optics Electron.* **2000**, *10*, 169–175. (d) Kodas T. T.; Hampden-Smith, M. J. *Aerosol Processing of Materials*; Wiley: New York, 1999. (e) Hubert-Pfalzgraf, L. G.; Guillon, H. *Appl. Organomet. Chem.* **1998**, *12*, 221–236. (f) Roger, C.; Corbitt, T.; Xu, C.; Zeng, D.; Powell, Q.; Chandler, C. D.; Nyman, M.; Hampden-Smith, M. J.; Kodas, T. T. *Nanostruct. Mater.* **1994**, *4*, 529–35.

(13) (a) Edwards, D. A.; Mahon, M. F.; Molloy, K. C.; Ogrodnik, V. *J. Mater. Chem.* **2003**, *13*, 563–570. (b) Edwards, D. A.; Harker, R. M.; Mahon, M. F.; Molloy, K. C. *Inorg. Chim. Acta* **2002**, *328*, 134–146. (c) Xu, C.; Hampden-Smith, M. J.; Kodas, T. T. *Chem. Mater.* **1995**, *7*, 1539–1546.

(14) (a) Lu, C. C.; Peters, J. C. *Inorg. Chem.* **2006**, *45*, 8597–8607. (b) MacBeth, C. E.; Thomas, J. C.; Betley, T. A.; Peters, J. C. *Inorg. Chem.* **2004**, *43*, 4645–4662. (c) Daida, E. J.; Peters, J. C. *Inorg. Chem.* **2004**, *43*, 7474–7485. (d) Jenkins, D. M.; Di Bilio, A. J.; Allen, M. A.; Betley, T. A.; Peters, J. C. *J. Am. Chem. Soc.* **2002**, *124*, 15336–15350.

(15) Pangborn, A. B.; Giardello, M. A.; Grubbs, R. H.; Rosen, R. K.; Timmers, F. J. *Organometallics* **1996**, *15*, 1518–20.

(16) Peters, J. C.; Feldmann, J. D.; Tilley, T. D. *J. Am. Chem. Soc.* **1999**, *121*, 9871–9872.

(17) Fraenkel, G.; Winchester, W. R. *Organometallics* **1989**, *8*, 2308–2311.

(18) Betley, T. A.; Peters, D. M. *Inorg. Chem.* **2003**, *42*, 5074–5084.

The solvent was removed in vacuo, giving 1.50 g (83% yield) of pale-yellow microcrystalline powder **1**. ^{1}H NMR (400.2 MHz, THF-d_8): δ 7.48 (d, 2H, *ortho-Ph*B), 7.26 (m, 12H, PhB(CH_2P *Ph*$_2$)$_3$), 7.10 (m, 18H PhB(CH_2P *Ph*$_2$)$_3$), 6.87 (m, 2H, *meta-Ph*B), 6.46 (t, 1H, *para-Ph*B), 1.92 (dq, 6H, PC H_2CH_3), 1.35 (s, 6H, PhB(C H_2PPh_2)$_3$), 1.21 (dt, 9H, PCH_2C H_3). ^{13}C NMR (100.6 MHz, THF-d_8): δ 147.22, 141.39, 132.62, 132.56, 132.53, 132.47, 131.06, 127.79, 127.70, 19.15 (P(CH_2CH_3)$_3$), 8.34 (P(CH_2 CH_3)$_3$). ^{31}P NMR (162.0 MHz, THF- d_8, 25 °C): δ −1.15 (dd, ^{1}J(P-^{109}Ag) = 216.92 Hz, ^{1}J(P-^{107}Ag) = 188.41 Hz, ^{2}J(P-P) = 30.94 Hz), −4.25 (dq, ^{1}J(P-^{109}Ag) = 463.00 Hz, ^{1}J(P-^{107}Ag) = 401.77 Hz, ^{2}J(P-P) = 30.94 Hz). ^{31}P NMR (162.0 MHz, THF- d_8, −103 °C): δ −1.64 (dd, ^{1}J(P-^{109}Ag) = 218.17 Hz, ^{1}J(P-^{107}Ag) = 189.99 Hz, ^{2}J(P-P) = 25.76 Hz), −2.51 (dq, ^{1}J(P-^{109}Ag) = 465.91 Hz, ^{1}J(P-^{107}Ag) = 405.97 Hz, ^{2}J(P-P) = 25.76 Hz). Anal. Calcd for $C_{51}H_{56}AgBP_4$: C, 67.20; H, 6.19; P, 13.59. Found: C, 67.23; H 6.27; P, 13.44.

Synthesis of [Li(TMEDA)^{n}BuB(CH_2PPh_2)$_3$]. To a stirring suspension of 7.08 g (22.0 mmol) Ph_2PCH_2Li·TMEDA in 45 mL of ether, cooled to −78 °C in an acetone/dry ice bath, was slowly added 7.3 mL of a 1.0 M hexane solution of ^{n}BuBCl$_2$. The cooling bath was then removed and the reaction mixture was allowed to warm to room temperature with stirring, during which time a colorless solid began to precipitate from the yellow solution. The solution was next filtered and the solvent removed in vacuo, affording a thick yellow oil. The oil was washed with 3 × 60 mL of pentane (vigorous stirring). The resulting solid residue was then dissolved in 60 mL of toluene and the resulting yellow solution filtered from the colorless solids via cannula. The solvent was removed in vacuo, giving 4.56 g (79% yield) of a deep-yellow microcrystalline powder. ^{1}H NMR (400.2 MHz, THF- d_8): δ 7.31 (m, 12H, ^{n}BuB(CH_2P *Ph*$_2$)$_3$), 7.01 (m, 18H, ^{n}BuB(CH_2P *Ph*$_2$)$_3$), 2.31 (s, 4H, Me_2NC H_2C H_2NMe_2), 2.16 (s, 12H, *Me*$_2$$NCH_2CH_2N$ *Me*$_2$, 1.30 (t, 2H, $CH_3CH_2CH_2C$ H_2B), 0.98 (s, 6H, ^{n}BuB(C H_2PPh_2)$_3$), 0.78 (m, 4H, CH_3C H_2C H_2CH_2B), 0.56 (t, 3H, C $H_3CH_2CH_2CH_2$B). ^{13}C NMR (100.6 MHz, THF- d_8): δ 135.8, 133.1, 132.5, 131.7, 55.2 (Me_2N *C*H_2 *C*H_2NMe_2), 42.7 (*Me*$_2$$NCH_2CH_2N$ *Me*$_2$), 22.6, 18.4, 15.8, 8.1. ^{31}P NMR (162.0 MHz, THF- d_8): δ −7.99 (s). Anal. Calcd for $C_{49}H_{61}BLiN_2P_3$.: C, 74.62; H, 7.80; P, 11.78. Found: C, 74.71; H, 7.55; P,11.79.

Synthesis of [^{n}BuB(CH_2PPh_2)$_3$Ag(PEt$_3$)] (2). Using a mortar and pestle, 0.83 g (5.8 mmol) AgCl was ground to a fine powder and added to a 100 mL flask containing 4.56 g (5.8 mmol) [Li(TMEDA)^{n}BuB(CH_2PPh_2)$_3$]. The flask was evacuated and backfilled with N_2 three times, covered with aluminum foil, and cooled to −78 °C in an acetone/dry ice bath. With stirring, tetrahydrofuran (45 mL) was added via syringe, followed by 0.85 g (5.8 mmol) of triethylphosphine. The reaction mixture was stirred for 30 min, then the flask was removed from the cooling bath and allowed the reaction mixture to warm to room temperature with stirring. The yellow solution was next separated from the colorless solids via cannula filtration into another Schlenk flask. The solvent was removed in vacuo and the resulting solids washed with 3 × 60 mL pentane (vigorous stirring) to facilitate TMEDA removal. The solid residue was then extracted with 60 mL dichloromethane. The yellow solution was filtered from the colorless solids via cannula filtration. The solvent was removed from the filtrate in vacuo, giving 4.07 g (79% yield) of a yellow powder (**2**). ^{1}H NMR (400.2 MHz, THF-d_8): δ 7.21 (m, 12H, ^{n}BuB(CH_2P *Ph*$_2$)$_3$), 6.99 (m, 18H ^{n}BuB(CH_2P *Ph*$_2$)$_3$), 1.87 (dq, 6H, PC H_2CH_3), 1.35 (s, 6H, ^{n}BuB(C H_2PPh_2)$_3$), 1.30 (t, 2H, $CH_3CH_2CH_2C$ H_2B) 1.16 (dt, 9H, PCH_2C H_3), 0.99 (m, 4H, CH_3C H_2C H_2CH_2B), 0.34 (t, 3H, C $H_3CH_2CH_2CH_2$B). ^{13}C NMR (100.6 MHz, THF-d_8): δ 142.2, 133.4, 130.7, 129.7, 128.5, 30.5, 28.7, 20.0, 18.4 (P(CH_2CH_3)$_3$), 9.4 (P(CH_2 CH_3)$_3$). 7.6. ^{31}P NMR (162.0 MHz, THF- d_8, 25 °C): δ −0.80 (dd, ^{1}J(P-^{109}Ag) = 206.71 Hz, ^{1}J(P-^{107}Ag) = 179.88 Hz, ^{2}J(P-P) = 30.57 Hz), −4.59 (dq, ^{1}J(P-^{109}Ag) = 464.09 Hz, ^{1}J(P-^{107}Ag) = 402.51 Hz, ^{2}J(P-P) = 32.24 Hz),. ^{31}P NMR (162.0 MHz, THF- d_8, −103 °C): δ −1.47 (dd, ^{1}J(P-^{109}Ag) = 215.06 Hz, ^{1}J(P-^{109}Ag) =186.62 Hz, ^{2}J(P-P) = 32.24 Hz), −2.94 (dq, ^{1}J(P-^{109}Ag) = 466.02 Hz, ^{1}J(P-^{107}Ag) = 406.94 Hz, ^{2}J(P-P) = 30.68 Hz). Anal. Calcd for $C_{49}H_{60}AgBP_4$: C, 66.01; H, 6.78; P, 13.90. Found: C, 65.96; H, 6.80; P, 13.66.

Synthesis of [Li(TMEDA)-PhB($CH_2P^iPr_2$)$_3$]. A stirring suspension of 5.0 g (36.2 mmol) of ^{i}Pr$_2$$PCH_2Li$ in 45 mL of ether and 5.43 mL (36.2 mmol) of anhydrous TMEDA was cooled to −78 °C in a acetone/dry ice bath. Next 1.62 mL (12.1 mmol) $PhBCl_2$ was slowly added. The cooling bath was then removed and the solution was allowed to warm to room temperature with stirring, during which time colorless solids precipitated from the orange solution. The solution was then filtered and the solvent removed from the filtrate in vacuo, affording a thick orange oil. The oil was then washed with 3 × 60 mL pentane (vigorous stirring) affording 7.16 g (88% yield) of an orange oil upon drying in vacuo. ^{1}H NMR (400.2 MHz, THF- d_8): δ 7.63 (d, 2H, *ortho-Ph*B), 6.86 (m, 2H, *meta-Ph*B), 6.78 (t, 1H, *para-Ph*B), 2.31 (s, 4H, Me_2NC H_2C H_2NMe_2), 2.16 (s, 12H, *Me*$_2$$NCH_2CH_2N$ *Me*$_2$, 1.43 (s, 6H, PhB(C H_2P ^{i}Pr$_2$)$_3$), 1.04 (m, 3H, PhB(CH_2P(C HMe$_2$)$_2$)$_3$), 0.83 (d, 36H, P(CH(C H_3)$_2$)$_2$). ^{13}C NMR (100.6 MHz, THF- d_8): δ 135.6, 135.0, 130.0, 127.7, 127.1, 57.0 (Me_2N *C*H_2 *C*H_2NMe_2), 44.1 (*Me*$_2$$NCH_2CH_2N$ *Me*$_2$), 25.0, 14.7. ^{31}P NMR (162.0 MHz, THF-d_8): δ −9.91. Anal. Calcd for $C_{33}H_{69}BLiN_2P_3$: C, 65.56; H, 11.50; P, 15.37. Found: C, 65.48; H, 11.46; P, 15.20.

Synthesis of [PhB($CH_2P^iPr_2$)$_3$Ag(PEt$_3$)] (3). Using a mortar and pestle, we ground 1.65 g (11.6 mmol) of AgCl to a fine powder and added it to a 100 mL flask containing 6.98 g (11.6 mmol) of [Li(TMEDA)PhB($CH_2P^iPr_2$)$_3$]. The flask was evacuated and backfilled with N_2 three times, covered with aluminum foil, and cooled with stirring to −78 °C in an acetone/dry ice bath. Next, tetrahydrofuran (45 mL) was added via syringe, followed by 1.70 g (11.6 mmol) of triethyl-phosphine. The reaction mixture was stirred for 30 min, and the flask was then removed from the cooling bath and allowed to warm to room temperature with stirring. The orange supernatant solution was then separated from the colorless solids via cannula filtration into another Schlenk flask, and the solvent was removed in vacuo. The resulting solid was washed with 3 × 60 mL pentane (vigorous stirring) to remove TMEDA, the solid residue was then extracted with 60 mL dichloromethane, and the resulting orange solution was filtered via cannula. The solvent was removed in vacuo, affording 6.03 g (74% yield) of an orange oil (**3**). ^{1}H NMR (400.2 MHz, THF-d_8): δ 7.71 (d, 2H, *ortho-Ph*B), 7.19 (m, 2H, *meta-Ph*B), 6.61 (t, 1H, *para-Ph*B), 1.96 (m, 6H, PC H_2CH_3), 1.68 (m, 9H, PCH_2C H_3), 1.21 (m, 3H, PhB(CH_2(P(C HMe$_2$)$_2$)$_3$), 1.16 (s, 6H, PhB(C H_2P ^{i}Pr$_2$)$_3$), 0.89 (d, 36H, P(CH(C H_3)$_2$)$_2$). ^{13}C NMR (100.6 MHz, THF-d_8): δ 135.4, 134.4, 127.3, 126.8, 125.0, 24.4, 19.7, 18.1 (P(CH_2CH_3)$_3$), 9.5 (P(CH_2 CH_3)$_3$). ^{31}P NMR (162.0 MHz, THF-d_8, 25 °C): δ 11.66 (br s, $\Delta\upsilon_{1/2}$ = 33.78 Hz), 2.30 (br s, $\Delta\upsilon_{1/2}$ = 44.62 Hz). ^{31}P NMR (162.0 MHz, THF-d_8, −103 °C): δ 8.21 (dd, ^{1}J(P-^{109}Ag) = 486.08 Hz, ^{1}J(P-^{107}Ag) = 425.33 Hz, ^{2}J(P-P) = 33.26 Hz), −1.02 (dq, ^{1}J(P-^{109}Ag) = 602.65 Hz, ^{1}J(P-^{107}Ag) = 528.20 Hz, ^{2}J(P-P) = 33.26 Hz). Anal. Calc. for $C_{33}H_{68}AgBP_4$: C, 56.02; H, 9.69; P, 17.51. Found: C, 56.01; H, 9.84; P, 17.78.

Synthesis of [Li(TMEDA)^{n}BuB($CH_2P^iPr_2$)$_3$]. To a stirring suspension of 1.90 g (13.8 mmol) ^{i}Pr$_2$$PCH_2Li$ in 45 mL of ether was added 2.07 mL (13.8 mmol) anhydrous TMEDA. The mixture was cooled to −78 °C in an acetone/dry ice bath with stirring, and 4.6 mL (4.6 mmol) of a hexane solution of ^{n}BuBCl$_2$ was slowly

added. The cooling bath was then removed and the solution was allowed to warm to room temperature with stirring, during which time a colorless solid precipitated from the yellow solution. The solution was then filtered via cannula and the solvent removed in vacuo, affording 1.84 g (86% yield) of a yellow solid. ^{1}H NMR (400.2 MHz, THF-d_8): δ 2.31 (s, 4H, Me_2NC H_2C H_2NMe_2), 2.16 (s, 12H, $Me_2NCH_2CH_2N$ Me_2, 1.47 (t, 2H, $CH_3CH_2CH_2C$ H_2B), 1.36 (m, 3H, ^{n}BuB($CH_2P(C$ $HMe_2)_2)_3$), 1.22 (s, 6H, ^{n}BuB(C H_2P ^{i}Pr$_2)_3$), 0.90 (d, 36H, P(CH(C $H_3)_2)_2$), 0.70 (m, 4H, CH_3C H_2C H_2CH_2B), 0.34 (t, 3H, C $H_3CH_2CH_2CH_2B$). ^{13}C NMR (100.6 MHz, THF-d_8): δ 56.2 (Me_2N CH_2 CH_2NMe_2), 43.3 ($Me_2NCH_2CH_2N$ Me_2), 26.6, 21.5, 17.6, 15.8, 14.1, 7.8. ^{31}P NMR (162.0 MHz, THF-d_8): δ −7.53. Anal. Calcd for $C_{31}H_{73}BLiN_2P_3$: C, 63.69; H, 12.59; P, 15.89. Found: C, 63.76; H, 12.26; P, 16.05.

Synthesis of [^{n}BuB($CH_2P^iPr_2)_3$Ag(PEt_3)] (4). Using a mortar and pestle, 0.56 g (3.9 mmol) AgCl was ground to a fine powder and added to a 100 mL flask containing 1.84 g (3.9 mmol) of [Li(TMEDA)^{n}BuB($CH_2P^iPr_2)_3$]. The flask was evacuated and backfilled with N_2 three times, covered with aluminum foil, and cooled to −78 °C with stirring in an acetone/dry ice bath. Next, tetrahydrofuran (45 mL) was added via syringe, followed by 0.58 g (3.9 mmol) triethylphosphine. The reaction mixture was stirred for 30 min., and then the flask was removed from the cooling bath and allowed to warm to room temperature with stirring. The yellow solution was separated from colorless solids via cannula filtration into another Schlenk flask, and the solvent was removed in vacuo. The resulting solid was then washed with 3 × 60 mL pentane (vigorous stirring) to remove TMEDA. The solid residue was then dissolved in 45 mL of dichloromethane and the resulting yellow solution was filtered from colorless solids via cannula filtration. The solvent was removed from the filtrate in vacuo, giving 1.82 g (68% yield) of a thick yellow oil (**3**). ^{1}H NMR (400.2 MHz, THF-d_8): δ 1.90 (m, 6H, PC H_2CH_3), 1.62 (m, 9H, PCH_2C H_3), 1.49 (t, 2H, $CH_3CH_2CH_2C$ H_2B), 1.40 (m, 3H, ^{n}BuB($CH_2P(C$ $HMe_2)_2)_3$), 1.25 (s, 6H, ^{n}BuB(C H_2P ^{i}Pr$_2)_3$), 1.03 (d, 36H, P(CH(C $H_3)_2)_2$), 0.78 (m, 4H, CH_3 $CH_2CH_2CH_2B$), 0.44 (t, 3H, C $H_3CH_2CH_2CH_2B$). ^{13}C NMR (100.6 MHz, THF-d_8): δ 27.6, 20.0, 19.1 ($P(CH_2CH_3)_3$), 17.2, 16.1, 15.2, 14.1, 8.0 ($P(CH_2$ $CH_3)_3$), 7.4. ^{31}P NMR (162.0 MHz, THF-d_8, 25 °C): δ 14.57 (br dd), 3.49 (br dq). ^{31}P NMR (162.0 MHz, THF-d_8, −103 °C): δ 11.53 (dd, ^{1}J(P-^{109}Ag) = 708.45 Hz, ^{1}J(P-^{107}Ag) = 617.27 Hz, ^{2}J(P-P) = 44.19 Hz), 4.35 (dq, ^{1}J(P-^{109}Ag) = 726.25 Hz, ^{1}J(P-^{107}Ag) = 629.53 Hz, ^{2}J(P-P) = 44.19 Hz). Anal. Calcd for $C_{31}H_{72}AgBP_4$: C, 54.16; H, 10.56; P, 18.02. Found: C, 54.25; H, 10.58; P, 17.87.

X-ray Single Crystal Diffraction Characterization of Complexes 1 and 2. Pale yellow crystals of [$PhB(CH_2PPh_2)_3Ag(PEt_3)$] (**1**) suitable for X-ray analysis were grown by slow cooling of a toluene solution to −40 °C. Slow cooling of a diethyl ether solution to −40 °C produced pale yellow crystals of [^{n}BuB($CH_2PPh_2)_3$-$Ag(PEt_3)$] (**2**) suitable for X-ray analysis. X-ray diffraction data were collected for single crystals of complexes **1** and **2** on a SMART-1000 CCD area detector instrument at 153(2) K with graphite monochromated Mo Kα X-ray radiation. Data were corrected for Lorentz and polarization effects. The structures were solved by direct methods and expanded using Fourier techniques. All nonhydrogen atoms were refined anisotropically. All calculations were performed using the Bruker SHELXTL crystallographic software. The higher *R* value for complex **2** is attributed to increased thermal disorder associated with the ^{n}Bu alkyl group and the triethylphosphine ethyl groups. Relevant data collection parameters are summarized in Table S1 of the Supporting Information.

Film Growth and Characterization. Thin films of metallic Ag were grown in a horizontal cold-wall quartz reactor with liquid aerosol injection and at atmospheric pressure (740–760 Torr) with a solvent trap and bubbler for the exhaust gas. Precursor solutions were nebulized with a TSI 3076 collision-type nebulizer and were deposited on substrates downstream in the reactor. Carrier gas (Ar) flow rates were controlled at 1.65 L/min with a mass flow controller. The 52100 steel for substrates was purchased from McMaster-Carr, then cut into 1 cm × 1 cm squares and polished to ∼20 nm roughness as determined by atomic force microscopy. The 1″ × 1″ 1737F Corning glass substrates were purchased from Precision Glass and Optics. MgO(100) (1 cm × 1 cm) substrates were purchased from MTI Corporation. Substrates were cleaned with acetone, then placed on the graphite susceptor in the AACVD reactor, and heated during film growth with an infrared lamp. The reactor was evacuated and backfilled with Ar three times prior to use, and the precursor reservoir loaded with freshly prepared precursor solutions in tetrahydrofuran (c = 0.015 mol/L) via cannula filtration (Whatman GF/B glass fiber filters). Susceptor temperatures were varied from 250–550 °C to determine optimum growth temperatures. Film thicknesses were measured with a Tencor P-10 profilometer and film chemical compositions were assayed with an Omicron ESCA Al Kα probe X-ray photoelectron spectrometer. Samples were sputtered with an Ar^+ ion beam before spectra were recorded. The phase purity of the Ag films was also examined using $\theta-2\theta$ scans on a computer-interfaced Rigaku DMAX-A powder diffractometer using Ni-filtered Cu Kα radiation, and glancing X-ray diffraction (GXRD; angle of incidence $\alpha = 0.3°$) $\theta-2\theta$ scans were recorded on a computer-interfaced Rigaku ATX-G diffractometer. Film microstructure and morphologies were assessed with an FEI Quanta 600sFEG scanning electron microscope and a Veeco TM CP II research atomic force microscope operating in the contact mode. Four-probe resistivity data were acquired on a Bio-Rad HL5500 instrument at room temperature.

Results

In this section, the synthesis of a new series of tris(phoshino)borato silver(I) AACVD precursors is presented, as well as a discussion of molecular structure and volatility characteristics. Next, two of these precursors are selected for thin film growth of metallic silver thin films on glass, MgO(100), and steel substrates, and their subsequent compositional and microstructural analysis is presented.

AACVD Precursor Synthesis and Characterization. Four tris(phosphino)borato silver(I) complexes, in which substituents on the boron and phosphorus atoms are varied from phenyl to alkyl groups, were synthesized in a three-step procedure (Scheme 1) modified from that of Peters et al.,[14] using commercially available reagents. Because of the light sensitivity of AgCl, its reaction with lithiated tris(phosphoryl)borate and PEt_3 was performed under aluminum foil. However, the subsequently formed new silver complexes are found to be air- and light-stable.

For complexes **1** and **2**, ^{31}P NMR spectroscopy indicates that exchange of the phosphine ligands is sufficiently slow at room temperature on the NMR time scale to give detectable ^{31}P−^{107,109}Ag spin–spin coupling. However, the ^{31}P NMR spectra of complexes **3** and **4** at room temperature show broadened peaks for the two distinct phosphorus chemical environments in the structure (tripodal ligand and PEt_3). Thus, low temperature (−103 °C) ^{31}P spectra were recorded in THF-d_8 for all complexes, and their coupling

Scheme 1. Three-step synthesis of complexes **1**–**4**

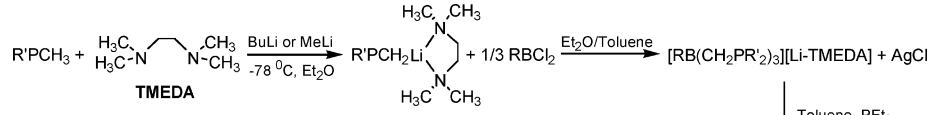

Complex		R	R'
$[PhB(CH_2PPh_2)_3Ag(PEt_3)]$	**1**	Ph	Ph
$[^nBuB(CH_2PPh_2)_3Ag(PEt_3)]$	**2**	^{n}Bu	Ph
$[PhB(CH_2P^iPr_2)_3Ag(PEt_3)]$	**3**	Ph	^{i}Pr
$[^nBuB(CH_2P^iPr_2)_3Ag(PEt_3)]$	**4**	^{n}Bu	^{i}Pr

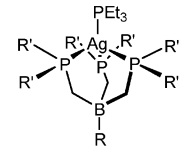

Table 1. Low-temperature (−103 °C) ^{31}P NMR Coupling Constant and Chemical Shift Data for Tripodal Ligand Skeletal Phosphorus (P_L) and Triethylphosphine Phosphorus (P_T) nuclei

	1	**2**	**3**	**4**
$^1J(^{109}Ag\text{-}P_L)$, $^1J(^{107}Ag\text{-}P_L)$ (Hz)	218, 190	215, 187	486, 425	708, 617
$^1J(^{109}Ag\text{-}P_T)$, $^1J(^{107}Ag\text{-}P_T)$ (Hz)	466, 406	466, 407	603, 528	726, 630
^2J(P-P) (Hz)	25.8	30.7	33.3	44.2
δ (ppm)	−1.64, −2.51	−1.47, −2.94	8.21, −1.02	11.53, 4.35

Table 2. Selected Bond Distances (Å) and Bond Angles (deg) for Complexes **1** and **2**

bond distances (Å)			bond angles (deg)		
bond	complex 1	complex 2	bond	complex 1	complex 2
Ag(1)−P(1)	2.4065(8)	2.439(2)	P(1)−Ag−P(2)	124.47(2)	124.04
Ag(1)−P(2)	2.5426(7)	2.551(2)	P(1)−Ag−P(3)	125.19(3)	125.59
Ag(1)−P(3)	2.5275(7)	2.512(2)	P(1)−Ag−P(4)	127.58(3)	125.91
Ag(1)−P(4)	2.5321(7)	2.5287(19)	P(2)−Ag−P(3)	89.91(2)	90.03(6)
			P(2)−Ag−P(4)	89.31(2)	90.56(7)
			P(3)−Ag−P(4)	88.73(2)	89.73(7)

constants are summarized in Table 1. Pale yellow single crystals suitable for diffraction studies were obtained by slow cooling of toluene (**1**) or ether (**2**) solutions. The crystal structures (Figure 2) confirm the mononuclearity of the molecular structures, with distorted tetrahedral coordination geometries about the Ag^+ centers similar to the geometries found in other low-valence transition metal complexes.[14] Metrical parameters are summarized in Table 2. The angles between the phosphorylborate P−Ag vectors, P−Ag−P, range from 88.72(2) to 89.91(2)° in complex **1** and from 89.73(7) to 90.56(7)° in complex **2**. The angles between the Et_3P-Ag and phosphorylborate-Ag vectors range from 124.47(3) to 127.57(3)° in complex **1** and from 124.04(6) to 125.91(7)° in complex **2**, indicating significant distortions from idealized tetrahedra. The Ag−P(phosphorylborate) bond lengths in complex **1** range from 2.5275(7) to 2.5426(7) Å. The Ag−PEt_3 bond length for the triethylphosphine P is shorter, at 2.4065(8) Å. In complex **2**, the Ag−P(phosphorylborate) bond lengths range from 2.512(2) to 2.551(2) Å. The Ag−PEt_3 bond length for the triethylphosphine P in complex **2** is 2.439(2) Å. Compared to the AgP_4 tetrahedra present in Ag_3P_{11} (P−Ag = 2.535(3) Å),[19] the only other reported Ag(I) compound surrounded by four P ligands, the Ag−P(phosphorylborate) bond lengths present in complexes **1** and **2** agree well (Figure 3). The Ag-PEt_3 distances in complexes **1** and **2** agree well with another solid state structure that involves a four-coordinate Ag(I)−triethylphosphine bond, $[Et_3PAgBr]_4$, where P−Ag = 2.402(3) Å (Figure 4).[20]

Differences in the Ag-PEt_3 bond lengths between complexes **1** and **2** can be explained as arising from the different substituents on the borate ligand. The phenyl substituent in the aryltrialkylborate (**1**) results in better anionic charge delocalization as compared with the tetraalkylborate in complex **2**. Hence, a stronger Coulombic interaction within the zwitterionic complex **2** between borate anion and silver cation can be anticipated, given the fact that the Ag-B distance is only slightly larger than the sum of the Ag and B van-der-Waals radii (3.42 Å).[21]We speculate that this ionic interaction may account for a stronger bond between Ag^+ and the PEt_3 ligand in complex **1**, resulting in a shorter Ag−PEt_3 bond length. This picture is supported by the greater Ag−B interatomic distance in complex **1** (3.656(3)) vs complex **2** (3.619(9)) and the slightly larger Ag-P coupling constant with the PEt_3 ligand found for complex **1** in the solution NMR (218 Hz (**1**), 215 Hz (**2**)). Likewise, Peters has recently interpreted spectroscopic results within a series of zwitterionic platinum and rhodium boratocomplexes in terms of Coulombic metal-borato interactions at similar M−B distances.[22]

Atmospheric pressure thermogravimetric analysis (TGA) scans for complexes **1**–**4** under N_2 are compared in Figure

(19) Moller, M. H.; Jeitschko, W. *Inorg. Chem.* **1981**, *20*, 828–833.

(20) Churchill, M. R.; Donahue, J.; Rotella, F. J. *Inorg. Chem.* **1976**, *11*, 2752–2758.

(21) Bondi, A. *J. Phys. Chem.* **1964**, *68*, 441.

(22) (a) Betley, T. A.; Peters, J. C. *Angew. Chem., Int. Ed.* **2003**, *42*, 2385. (b) Thomas, C. M.; Peters, J. C. *Organometallics* **2005**, *24*, 5858.

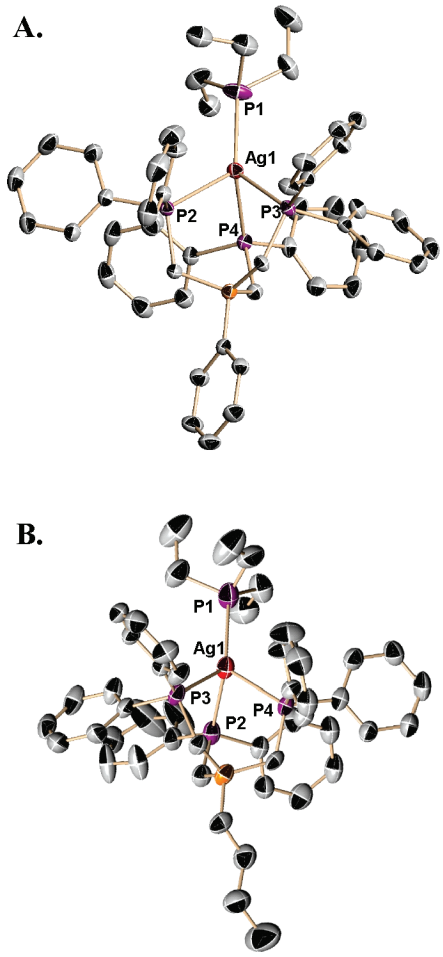

Figure 2. ORTEP drawings (ellipsoids at the 50% confidence level) of (A) [PhB(CH_2PPh_2)$_3$Ag(PEt_3)] (**1**) and (B) [^{n}BuB(CH_2PPh_2)$_3$Ag(PEt_3)] (**2**) molecular structures showing the Ag and P atom labeling schemes. Hydrogen atoms are omitted for clarity.

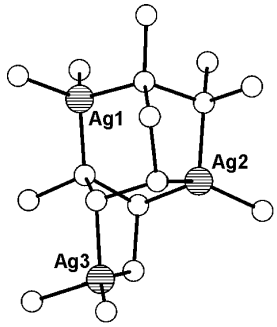

Figure 3. Core structure of Ag_3P_{11}. Reprinted with permission from ref 19. Copyright 1981 American Chemical Society.

5. Complex **1** shows the most abrupt weight loss features, occurring in two distinct steps at 160 and 205 °C. The first decomposition step (−12.8%) corresponds to the calculated weight percent loss for triethylphosphine of −12.9%. The second decomposition step yields dark gray material with a residual weight percent of 15.3%. This can be compared to the calculated weight percentage for pure silver of 11.8%, where the additional 3.5% would then be attributable to decomposed ligand fragments. For the other complexes, the decomposition range for each complex is wider than for complex **1**, and final decompositions are at higher temperatures, again resulting in dark gray residues. Complex **2** exhibits the lowest residual weight percent (12.5%), which can be compared to the calculated weight percentage for pure silver of 12.0%, with the additional 0.5% attributable to decomposed ligand contamination. Complexes **3** and **4** give residual weights of 25.0 and 19.9%, respectively. These residual weights correspond to calculated weight percentages for silver of 15.1 and 15.6%, respectively. Again, the additional weight percentages appear to be due to decomposed ligand contamination (9.9 and 4.3%, respectively).

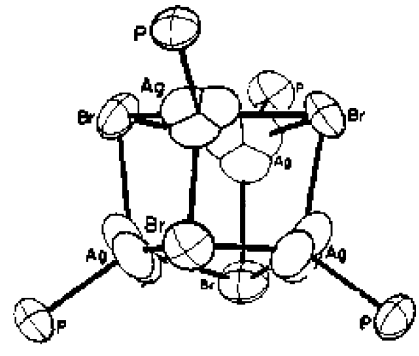

Figure 4. $P_4Ag_4Br_4$ core of [PEt_3AgBr]$_4$, showing 3-fold disorder of the silver atoms. Reprinted with permission from ref 20. Copyright 1976 American Chemical Society.

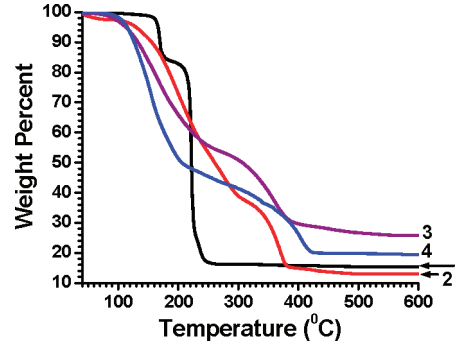

Figure 5. Atmospheric pressure thermogravimetric analysis (TGA) of the volatility characteristics of complexes **1**−**4**. The weight loss data were recorded at a ramp rate of 2.5 °Cmin^{-1} and 50 mL min^{-1} N_2 flow rate.

Ag Thin Film Growth and Characterization. Complex **1** was initially chosen for silver metal film growth process experiments on glass and Mg(100) (advanced interconnect applications), and 52100 steel substrates (lubricant coating applications) because of the sharp, two-step volatilization process determined by TGA. AACVD film growth was carried out with 0.015 M solutions of complex **1** in THF. The optimum susceptor temperature for high growth rates and crystallinity was found, with some experimentation, to be 300 °C. However, on glass and MgO(100) substrates, under these conditions, only minute quantities of transparent brown films are deposited. Glancing X-ray diffraction (GXRD) reveals the (111) and (200) reflections of cubic phase silver metal (PDF 04–0783, Figure 6) for the films grown on MgO(100). On 52100 steel, growth rates are 0.5–0.6 nm/min, depositing brown-tinted adherent films which are visibly reflective. The X-ray diffraction (XRD) $\theta-2\theta$ scan carried out on 100 nm films shows only reflections from polycrystalline iron (PDF 06–0696). However, X-ray photoelectron spectroscopy (XPS) does show the

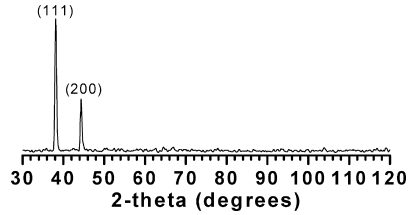

Figure 6. Glancing X-ray diffraction (GXRD) $\theta-2\theta$ scan ($\alpha = 0.30°$) of a Ag film grown on MgO(100) by AACVD using precursor **1**. Peaks are labeled with the corresponding (*hkl*) reflections from cubic phase Ag (PDF 04−0783).

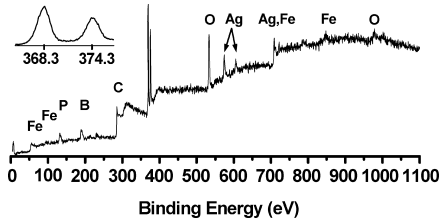

Figure 7. X-ray photoelectron spectroscopy (XPS) spectrum of a Ag film deposited on 52100 steel by AACVD using precursor **1**. Peaks are labeled with their corresponding element. The inset is enlarged portion of the spectrum showing the Ag $3d_{5/2}$ and $3d_{3/2}$ ionizations.

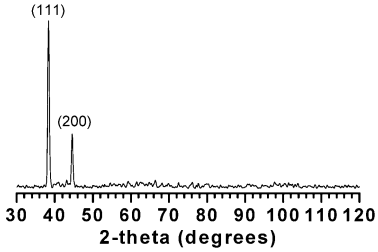

Figure 8. Glancing X-ray diffraction (GXRD) $\theta-2\theta$ scan ($\alpha = 0.30°$) of Ag film grown on MgO(100) by AACVD using precursor **2**. Peaks are labeled with the corresponding (*hkl*) reflections for cubic phase Ag (PDF 04−0783).

presence of metallic silver (Figure 7). The Ag $3d_{5/2}$ and $3d_{3/2}$ peak positions match precisely those of Ag metal.[23] However, other features are evident corresponding to 3% B, 9% C, 3% P versus Ag, as well as Fe and O attributable to the substrate.

Precursor **2** was next investigated for the growth of Ag films by AACVD, because of its cleaner decomposition characteristics in comparison to the other precursors as determined by the atmospheric pressure TGA experiments (Figure 5). As conducted for precursor **1**, AACVD growth was carried out with 0.015 M solutions of complex **2** in THF. For this precursor, the optimum temperature for conformal Ag film growth was determined to be 500 °C. The glass and Mg(100) substrates again yielded minute quantities of transparent gray/brown films. Thicknesses ranged between 25 and 30 nm for a 2.5 h growth time. GXRD reveals the same diffraction pattern as with precursor **1** with increased intensities (Figure 8). For 52100 steel as the substrate, a dark gray, reflective film was deposited at a growth rate of 14–18 nm/min. The XRD $\theta-2\theta$ scan carried out on 3 μm thick films (Figure 9) exhibits strong iron reflections, however the weak reflection at 38.1° can be assigned to the cubic phase

(23) *Handbook of X-ray Photoelectron Spectroscopy*; Chastain, J., King, R. C. Eds.; Physical Electronics: Eden Prairie, MN, 1995.

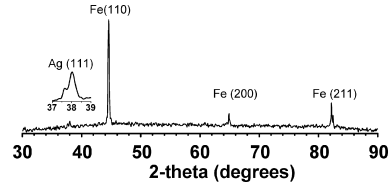

Figure 9. X-ray diffraction (XRD) $\theta-2\theta$ scan of Ag film grown on 52100 steel by AACVD using precursor **2**. Peaks are labeled with the corresponding (*hkl*) reflections from cubic phase Fe (PDF 06−0696) and cubic phase Ag (PDF 04−0783).

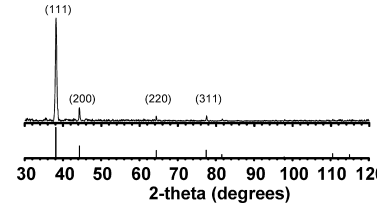

Figure 10. Glancing XRD $\theta-2\theta$ scan ($\alpha = 0.30°$) of Ag film grown on 52100 steel by AACVD using precursor **2**. Plotted underneath are the peak positions and relative intensities for the powder pattern of cubic phase Ag (PDF 04−0783).

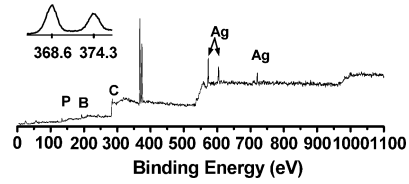

Figure 11. XPS spectrum of a Ag film deposited on 52100 steel by AACVD using precursor **2**. Peaks are labeled with their corresponding element. The inset is enlarged portion of the spectrum showing the Ag $3d_{5/2}$ and $3d_{3/2}$ ionizations.

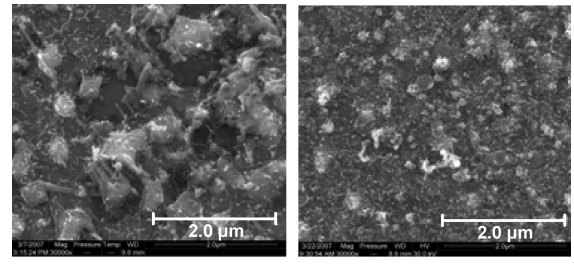

Figure 12. SEM images of Ag films grown on a 52100 steel substrate using precursor **2** with growth times of (A) 5 min and (B) 3.5 h.

of Ag. Furthermore, GXRD of these samples reveals reflections for polycrystalline cubic-phase Ag with slightly preferred orientation for the (111) direction (Figure 10). XPS also confirms the presence of Ag metal (Figure 11). Traces of contamination (1% B, 4% C, 1% P), doubtless arising from decomposed ligand are also detected, although at substantially lower levels than observed with precursor **1**. Absent from the XPS spectrum are features due to the underlying substrate (Fe, O).

The microstructure and the growth mechanism of the silver films were analyzed using scanning electron microscopy (SEM) and atomic force microscopy (AFM). Figure 12 shows SEM images of two films grown by AACVD using precursor **2**. In the first image (Figure 12A), growth of the silver films was conducted for 5 min under the conditions described above, revealing small (<100 nm) particles with little apparent ordering and incomplete coverage of the

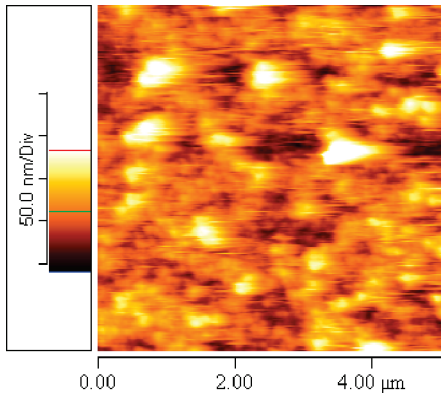

Figure 13. Atomic force microscopy scan of 5.0 μm × 5.0 μm of the Ag film shown in Figure 12B. R_{rms} = 55.4 nm; R_{p-v} = 463 nm.

substrate. The next image (Figure 12B) is of a silver film grown under the same conditions for a 3.5 h period. Here the substrate has full coverage by the Ag film with little ordering and significant apparent roughness as indicated by lighter shaded peaks rising from the film. AFM data (Figure 13) agree with this assessment, with an rms roughness (R_{rms}) of 55.4 nm and a peak-to-valley roughness (R_{p-v}) of 463 nm.

Charge transport measurements can provide a qualitative assessment of silver film quality, with measured resistivities that are closer to bulk silver indicating higher film quality/purity.[11a,24] Resistivities measured on the films grown for 3.5 h on 52100 steel (3 μm thick) were 2–3 $\mu\Omega$ cm, very close to the resistivity reported for bulk silver (1.6 $\mu\Omega$ cm).[25] The current flow on the bare 52100 steel substrates was below the instrumental detection limit.

Discussion

Precursor Design and Synthesis. The goal of this investigation was to design and realize efficient AACVD precursors for metallic silver thin films. Previous studies have relied on fluorinated precursor ligand substituents to provide ambient atmosphere stability and volatility. The complexes developed in the present study utilize a tridentate phosphinoborate ligand, along with a neutral ancillary triethylphosphine ligand, to securely saturate the metal ion coordination sphere. This results in a new series of silver complexes that are both light- and air-stable, as well as excellent AACVD precursors for metallic silver films.

An ideal AACVD precursor is soluble in common organic solvents, should have sufficient volatility to form aerosol particles capable of being delivered to the desired substrate,[26] and should decompose cleanly to the target material. The synthesis of complexes **1**–**4** is accomplished in three straightforward steps (Scheme 1), modified from a procedure developed in literature for other low-valent late transition metals,[16–18] using commercial reagents. This new family of precursors exhibits good solubility in a variety of common organic solvents (toluene, THF, ether, acetone, dichloromethane, pyridine).

The $^1J(^{107}Ag-^{31}P)$ parameters in tetrahedral silver complexes of tertiary phosphines generally range from 190 to 235 Hz,[27,28] with higher magnitudes found for phosphites[27a,29] and aminophosphines.[28] The low temperature (−103 °C) values for the $^1J(^{107}Ag-^{31}P_T)$ in complexes **1** (406 Hz) and **2** (407 Hz) are rather large for tetrahedral Ag(I) complexes and more closely match values associated with two- and three-coordinate Ag^+ phosphine complexes in solution. The $^1J(^{107}Ag-^{31}P_T)$ values for complexes **3** and **4** are also very large (528 and 630 Hz, respectively) for tetrahedral Ag(I) complexes and closer in range to one-coordinate Ag^+ phosphine complexes in solution. The ^{31}P NMR spectra patterns suggest that the solid state structures of complexes **1**–**4** are essentially maintained in solution. The ratios of the isotopomeric Ag-P coupling constants ($^1J(^{109}Ag-P)/^1J(^{107}Ag-P)$ = 1.14–1.15) are in excellent agreement with the theoretical ratio $\gamma(^{109}Ag)/\gamma(^{107}Ag)$ = 1.15. The resonance due to Et_3P is a pair of doublets owing to splitting by ^{107}Ag [I = ½; 51.82% natural abundance] and ^{109}Ag [I = ½; 48.18% natural abundance], and each component is further split into a 1:3:3:1 quartet by coupling to the three magnetically equivalent phosphorus nuclei of the tripodal ligand. The couplings are such that the patterns overlap, giving a 1:4:6:4:1 pattern for complexes **1** and **2**, and multiplets for complexes **3** and **4**. The tripodal ligand ^{31}P nuclei appear as a pair of doublet-of-doublets with ^{107}Ag and ^{109}Ag couplings, and a two-bond $^{31}P-^{31}P$ coupling to the triethylphosphine phosphorus. At low temperature (−103 °C), the resonances are generally sharper, owing to a decrease in the rate of ligand exchange.

Thermal analysis shows that by varying the ligand framework substituents, decomposition temperatures can be altered to provide cleanly decomposing precursors. Introduction of an alkyl substituent on the boron results in thermal decomposition products more closely approaching metallic Ag for complexes **2** and **4** vs complexes **1** and **3**, where there is a B-Ph substituent. When comparing alkyl vs phenyl phosphorus substitution on the tripodal ligand, the opposite trend is observed. Thus, thermal decomposition products of complexes **1** and **2** with phenyl-substituted phosphines more closely approach metallic Ag.

Of the four new precursors, complexes **1** and **2** were chosen for film growth experiments. Complex **1** displays a sharp decomposition temperature in the atmospheric pressure

(24) (a) Haase, T.; Kohse-Hoeinghaus, K.; Atakan, B.; Schmidt, H.; Lang, H. *Chem. Vap. Deposition* **2003**, *9*, 144–148. (b) Roger, C.; Corbitt, T. S.; Hampden-Smith, M. J.; Kodas, T. T. *Appl. Phys. Lett.* **1994**, *65*, 1021–1023.
(25) Smith, D. R.; Fickett, F. R. *J. Res. Nat. Inst. Stand. Technol.* **1995**, *100*, 119–171.
(26) (a) Ashraf, S.; Blackman, C. S.; Palgrave, R. G.; Naisbitt, S. C.; Parkin, I. P. *J. Mater. Chem.* **2007**, *17*, 3708–3713. (b) Ashraf, S.; Blackman, C. S.; Hyett, G.; Parkin, I. P. *J. Mater. Chem.* **2006**, *16*, 3575–3582.
(27) (a) Alyea, E. C.; Malito, J.; Nelson, J. H. *Inorg. Chem.* **1987**, *26*, 4294–4296. (b) Price, S. J. B.; Brevard, C.; Pagelot, A.; Sadler, P. J. *Inorg. Chem.* **1985**, *24*, 4278–4281. (c) Alyea, E. C.; Dias, S. A.; Stevens, S. *Inorg. Chim. Acta* **1980**, *44*, L203–L204. (d) Goel, R. G.; Pilon, P. *Inorg. Chem.* **1978**, *17*, 2876–2879. (e) Hollander, F. J.; Ip, Y. L.; Coucouvania, D. *Inorg. Chem.* **1976**, *15*, 2230–2234. (f) Muetterties, E. L.; Alegranti, C. W. *J. Am. Chem. Soc.* **1972**, *94*, 6386–6891.
(28) Socol, S. M.; Verkade, J. G. *Inorg. Chem.,* **1984**, *23*, 3487–3493.
(29) Colquhoun, I. J.; McFarlane, W. *J. Chem. Soc., Chem. Commun.* **1980**, *145*, 147.

TGA, whereas complex **2** decomposes to Ag relatively free of contamination. Complex **2** was found to provide higher growth rates and Ag film purity on steel substrates, thus proving to be the most effective precursor of the four complexes for the efficient growth of metallic Ag thin films.

Silver Film Growth and Characterization. Silver films were grown by AACVD using both precursors **1** and **2** on three different substrates, amorphous glass, single crystal cubic phase MgO (100), and polycrystalline 52100 steel (cubic phase iron). Only the (111) and (200) growth orientations are observed for the films grown on MgO(100) substrates, while more orientations are observed for films grown on 52100 steel. Other work has shown that substrate texture can significantly affect growth orientation in metallic silver films.[30] In the present study higher film growth rates are observed for films deposited on 52100 steel than for that on MgO(100) or amorphous glass. To the best of our knowledge, there have been no reports comparing substrate effects on Ag CVD film growth rates. One hypothesis is that the greater steel substrate surface roughness (~20 nm) vs the MgO(100) substrates (~5 nm) promotes nucleation, thus resulting in higher deposition rates. A recent study compared growth rate and substrate surface roughness in the electrocyrstallization of Ag on carbon electrodes, however found no direct correlation.[31] Better wetting of Ag on the ferrous steel substrate vs MgO might also be responsible for the observed increase in growth rate. Silver is known to wet oxide substrates poorly,[32] and adhesion and wetting of Ag has been shown to improve by adding transition metal interlayers.[33] In a study of carbonaceous deposits on iron substrates, it was concluded that the better surface wetting of the deposits on iron contributed to the observed higher growth rates and surface coverage.[34]

For Ag film growth on 52100 steel substrates with precursor **1**, the degree of decomposed ligand contamination (3% B, 9% C, 3% P, as determined from XPS) adversely affects film growth rate and crystallinity. However, precursor **2**, with a significantly lower degree of decomposed ligand contamination (1% B, 4% C, 1% P), can be used to deposit metallic silver films at higher growth rates with better surface coverage and higher crystallinity. An XRD $\theta-2\theta$ scan shows a small feature corresponding to the Ag (111) reflection, while GXRD reveals the full polycrystalline pattern for the cubic phase of silver in the films. The cubic phase is by far the most common phase for metallic Ag, although a metastable hexagonal phase is known.[35] XPS confirms that the present silver films are metallic Ag, from the position of the 3d photoelectron peaks, with shifting to higher binding energies expected for silver in higher oxidation states.[20] The resistivities of films grown with precursor **2** approach those of pure bulk Ag,[1a] suggesting that contamination is minimal.

The SEM and AFM images of the silver films grown with precursor **2**, measured after only 5 min (Figure 12A) of deposition and after 3.5 h (Figure 12B), provide information on the film growth mechanism. The first image (Figure 12A) shows small Ag particles on the steel substrate. After longer deposition times (Figure 12B), these "islands" have coalesced into a conformal film, relatively rough as evidenced by AFM (Figure 13). This island growth (Volmer–Weber) mechanism is a common mode of Ag film growth on oxide and semiconductor surfaces,[8d,36] because of weak interaction energies between the adsorbed metal atom and the substrate.

Conclusions

Four new light- and air-stable Ag(I) coordination complexes have been synthesized, characterized, and evaluated as potential AACVD precursors. Silver film growth has been demonstrated using complexes **1** and **2**, with the latter giving higher growth rates of silver films having electrical resistivities approaching that of bulk silver. Film growth is suggested to occur through an island growth that coalesces to conformal coverage. These complexes represent a significant improvement in nonfluorinated Ag precursors, offering ease of handling and efficient film deposition. While marginal wettability of the films on untreated amorphous glass and Mg(100) substrates makes application as interconnects unlikely, the conformal coverage on 52100 steel makes the Ag films grown in this study promising as solid lubricant coatings. Future studies will focus on the tribological characteristics of these films.

Acknowledgment. We thank the NSF (grant CMS-0510895) for support of this research, and the Northwestern Materials Research Center (NSF MRSEC grant DMR-0520513) for providing characterization facilities. We thank Prof. Q. Jane Wang for stimulating discussions about tribology, as well as Dr. Yuyang Wang for assistance with VTNMR data collection and Dr. J. Carsello for assistance with X-ray diffraction measurements. We also thank Mr. M. T. Russell for assistance with SEM image collection.

Supporting Information Available: Detailed crystallographic information for complexes **1** and **2**, room and low temperature ^{31}P NMR for all complexes and VT ^{31}P NMR for complex **3** (PDF). This material is available free of charge via the Internet at http://pubs.acs.org.

IC701852X

(30) (a) Zoo, Y.; Alford, T. L. *J. Appl. Phys.* **2007**, *101*, 0335051–0335056. (b) Yang, F.-L.; Somekh, R. E.; Greer, A. L. *Thin Solid Films* **1998**, *322*, 46–55.
(31) Miranda-Hernandez, M.; Gonzalez, I.; Batina, N. *J. Phys. Chem. B* **2001**, *105*, 4214–4223.
(32) (a) Campbell, T. C. *Surf. Sci. Rep.* **1997**, *27*, 1–111. (b) Chatain, D.; Coudurier, L.; Eustathopoulos, N. *Rev. Phys. Appl.* **1988**, *23*, 1055–1064.
(33) (a) Lazzari, R.; Jupille, J. *Phys. Rev. B* **2005**, *71*, 0454091–04540913. (b) Koestlmeier, S.; Elsaesser, C. *J. Phys.: Cond. Matter* **2000**, *12*, 1209–1222.
(34) Parke, B. L. *Lubr. Eng.* **1991**, *48*, 209–218.
(35) (a) Jona, F.; Marcu, P. M. *J. Phys.: Condens. Matter* **2004**, *16*, 5199–5204. (b) Taneja, P.; Banerjee, R.; Ayyub, P. *Phys. Rev. B* **2001**, *64*, 0334051–0334054.
(36) Venables, J. A.; Derrien, J.; Janssen, A. P. *Surf. Sci.* **1980**, *95*, 411–430.